Earth, Planets and Space

EXPRESS LETTER Open Access

Ionospheric disturbances observed over Japan following the eruption of Hunga Tonga-Hunga Ha'apai on 15 January 2022

Susumu Saito*

Abstract

Traveling ionospheric disturbances (TIDs) were observed over Japan by using Global Navigation Satellite System (GNSS) receiver network data after the eruption of Hunga Tonga-Hunga Ha'apai in Tonga on 15 January 2022. Two types of TIDs with different characteristics were observed as perturbation in the total electron content (TEC). The first one arrived at Japan which are located about 7800 km away from Hunga Tonga-Hunga Ha'apai about 3 h after the eruption. The amplitude was about ± 0.5 TECU. The wavefronts was in the NNE–SSW direction and propagated in the WNW direction (– 69° counter-clockwise from the north) at 250 m s^{-1}. The wavelength was estimated as 400 km. The second one arrived at Japan about 7 h after the eruption. The amplitude was about ± 1.0 TECU. The wavefronts was in the NE–SW direction and propagated in the NW direction (– 53° counter-clockwise from the north) at 270 m s^{-1}. The wavelength was longer than the first one and was estimated as 800 km. The first one were associated with ionospheric irregularities represented by the rate of TEC index (ROTI). In contrast, the second one did not have irregularities all over the TIDs, but in only a limited region. The arrival of the first TID was too early for the atmospheric acoustic waves to arrive, while the arrival of the second TIDs approximately coincided with the arrival of surface pressure enhancement. To understand the mechanisms of the TIDs, further studies with wide-area observations as well as numerical calculations are necessary. TIDs and ionospheric irregularities after volcanic eruption could be threats to GNSS-based systems especially for those which utilize carrier-phase measurements.

Keywords: Ionospheric traveling ionospheric disturbance, Volcano eruption, Ionospheric irregularities

*Correspondence: susaito@mpat.go.jp
Electronic Navigation Research Institute, National Institute of Maritime, Port and Aviation Technology, 7-42-23 Jindaiji-Higashi, Chofu, Tokyo 182-0012, Japan

Graphical Abstract

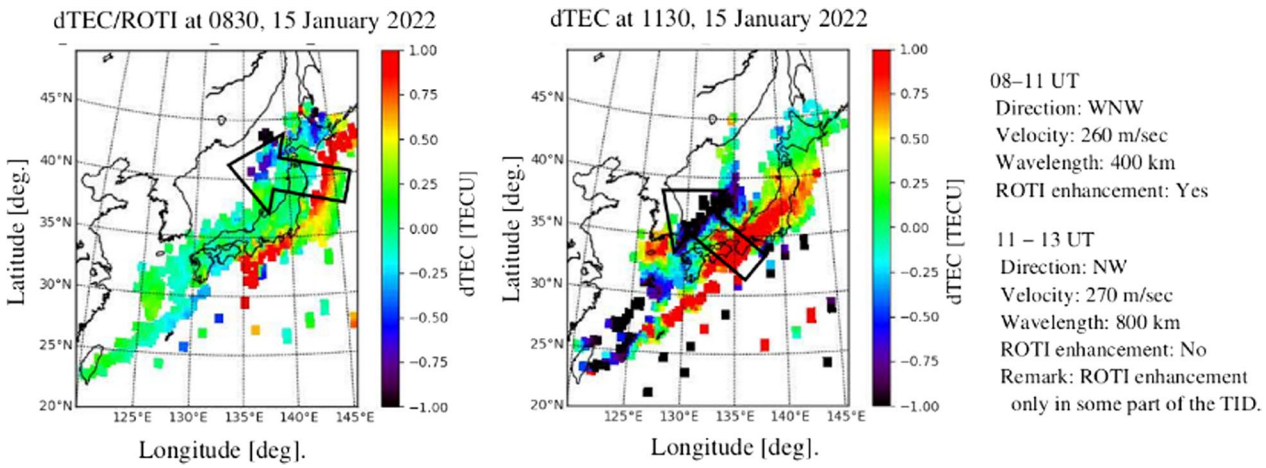

Introduction

It has been well known that sudden movement of the earth's surface causes atmospheric waves which propagate through the atmosphere to upper atmosphere, eventually causing traveling ionospheric disturbances (TIDs). Such TIDs have been observed associated with earthquake, tsunami, volcanic eruption, underground nuclear explosions and so on. Huge earthquakes generate atmospheric acoustic and gravity waves to cause TIDs (e.g., Afraimovich et al. 2001; Otsuka et al. 2006; Saito et al. 2011). Huge volcanic eruptions generate TIDs which travels very long distances. Ogawa et al. (1982) observed TIDs which were associated with the eruption of Mount St. Helens in 1980 at the west coast of US and propagated across the Pacific Ocean to Japan. Cheng and Huang (1992) observed TIDs associated with the eruption of Mount Pinatubo in 1991 in Philippines. Tsunamis are also known to emit atmospheric waves which propagates up to the ionosphere to cause TIDs. Savastano et al. (2017) suggested that TIDs could be utilized to remotesense the propagation of tsunamis. Underground nuclear explosions also generates TIDs (Park et al. 2014). They showed that TIDs associated with underground nuclear explosion could be distinguished from other types of TIDs by examining the waveform of the TIDs. Thus, the TIDs associated with the sudden motion of the earth's surface are interesting not only as responses of the ionosphere to atmospheric waves, but also as proxies to know the characteristics of the motion of the earth's surface.

These TIDs have been observed by different techniques. Ogawa et al. (1982) used the high-frequency Doppler sounding to detect oscillations of the ionosphere. Maruyama et al. (2012) and Maruyama and Shinagawa (2014) used the ionosonde to find characteristic signatures of ionograms. Nowadays, ionospheric total electron content (TEC) measurements by observing radio signals from the Global Navigation Satellite System (GNSS) satellites represented by the Global Positioning System (GPS) (e.g., Afraimovich et al. 2001; Otsuka et al. 2006). More recently, data from GNSS networks enabled us to visualize ionospheric disturbances as two-dimensional maps (Saito et al. 1998). Saito et al. (2011) and Tsugawa et al. (2011) visualized co-centric TIDs associated with the 2011 Tohoku-oki earthquake.

Hunga Tonga-Hunga Ha'apai (20.55° S, 175.39° W) in Tonga erupted around 0400 UTC on 15 January 2022. It was a huge eruption expanding volcanic clouds and waves in the atmosphere were observed also by meteorological satellites. Tsunamis were observed in Tonga. In Japan, in addition to sudden enhancements of the surface pressure was observed around 1130 UT along the pacific coast of Japan which is about 7 h after the eruption. Enhancements in the tide level were also observed by Japan Meteorological Agency (https://www.jma.go.jp/jma/press/2201/16a/kaisetsu202201160200.pdf, in Japanese). The enhancement in the tide level was assumed to be associated with the eruption. It was easily imagined that TIDs would be induced by the eruption of Hunga Tonga-Hunga Ha'apai and related phenomena.

The GNSS Earth Observation Network (GEONET) is a Japanese nationwide GNSS reference station network operated by the Geospatial Information Authority of Japan. It consists of about 1300 GNSS receivers. High-resolution ionospheric disturbance maps can be obtained by the data from the densely distributed GEONET

stations. Characteristics of ionospheric behaviors following the eruption of Hunga Tonga-Hunga Ha'apai were investigated by using data from a part of the GEONET stations.

Methods

Raw measurement data of Global Positioning System (GPS) satellites at a rate of 1 Hz from 200 stations of GEONET were used. Figure 1 shows the distribution of the 200 GEONET stations used in this study. Although GEONET can track GPS, GLONASS, Galileo, and Quasi-Zenith Satellite System (QZSS), only GPS satellites data were used to simplify the data processing.

The ionospheric TEC between a GPS satellite and a receiver were derived by the linear combination of carrier-phase measurements of GPS L1 and L2 signals at 1.57542 GHz and 1.22760 GHz, respectively, by the following equation:

$$\mathrm{TEC}_{\mathrm{obs}}(t) = 9.52(\phi_2(t) - \phi_1(t)), \tag{1}$$

where $\mathrm{TEC}_{\mathrm{obs}}(t)$ is the observed TEC in the unit of TECU (10^{16} electrons m^{-2}) at time t, and $\phi_1(t)$ and $\phi_2(t)$ are the carrier-phase measurements of the GPS L1 and L2 signals in the unit of meters, respectively. The carrier-phase measurements were used, because the measurement noises are much smaller than those of the code measurements. The derived TEC includes constant bias associated with the ambiguities in the carrier-phase measurements as well as the inter-frequency biases arising from the hardware delays in the satellite and receiver. Because the carrier-phase measurement noise is usually some millimeters, the TEC derived by the carrier-phase measurements has noise of less than 0.1 TECU.

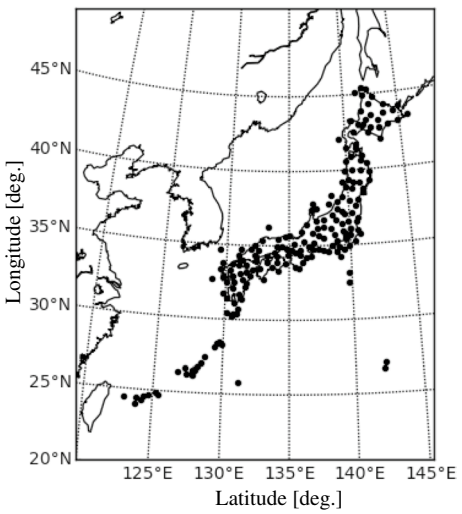

Fig. 1 Distribution of the 200 GEONET stations used in this study

The ionospheric disturbances are detected by deriving perturbation component of the TEC (or delta-TEC, dTEC) (Saito et al. 1998). By taking the perturbation component of the TEC, the biases in the derived TEC can be eliminated. dTEC is derived by

$$\mathrm{dTEC}(t) = \mathrm{TEC}_{\mathrm{obs}}(t) - \mathrm{TEC}_{\mathrm{pred}}(t), \tag{2}$$

where $\mathrm{TEC}_{\mathrm{pred}}(t)$ is the TEC at time t predicted by the third-order polynomial function fitted to the previous 1 h observation data (Maeda and Heki 2014; Saito et al. 2014). dTEC values are derived for each GPS satellite and GEONET receiver pairs. Assuming that the ionospheric perturbation exists mainly around the density peak of the F region, the derived dTEC values are mapped to the ionospheric pierce point (IPP) at an altitude of 350 km. The dTEC values are averaged over the grid of $0.25^\circ \times 0.25^\circ$ in latitude and longitude. dTEC maps are generated every 5 min in near real-time with 2 min latency (Saito et al. 2014).

To derive the ionospheric irregularities, the rate of TEC index (ROTI) (Pi et al. 1997) is used. The ROTI is defined as the standard deviation of temporal variation of the TEC as

$$\mathrm{ROT} = \frac{\mathrm{TEC}(t) - \mathrm{TEC}(t - \delta t)}{\delta t}, \tag{3}$$

$$\mathrm{ROTI} = \sqrt{\langle \mathrm{ROT} \rangle - \langle \mathrm{ROT} \rangle^2}, \tag{4}$$

where δt is the time step and "$\langle\rangle$" represents the ensemble average. We used 30 s for δt and the ensemble average are taken over the samples in 5 min. ROTI values are estimated for each GPS satellite and GEONET receiver pairs and mapped at the IPPs at an altitude of 350 km. ROTI maps are generated every 5 min in near real-time with 2-min latency (Saito et al. 2021).

Results and discussion

Figure 2 shows the series of dTEC maps over Japan from 0600 to 1500 UT [1500 to 2400 Japan Standard Time (JST)]. (A movie of the time evolution of the dTEC maps with 5-min time step is included in Additional file 1). It can be seen that there are traveling ionospheric disturbances (TIDs) with two different characteristics. At 0700 UT, ionospheric disturbances of dTEC amplitude of about ±0.5 TECU appeared from the east. The amplitude is comparable to those of typical TIDs over the mid-latitude region. The wave front was aligned in the NNE–SSW direction. To estimate the propagation velocity and wavelength more quantitatively, keograms of dTEC (time–distance plot of dTEC) were used to estimate the TID parameters. It helps reducing the effects of the geographical distributions

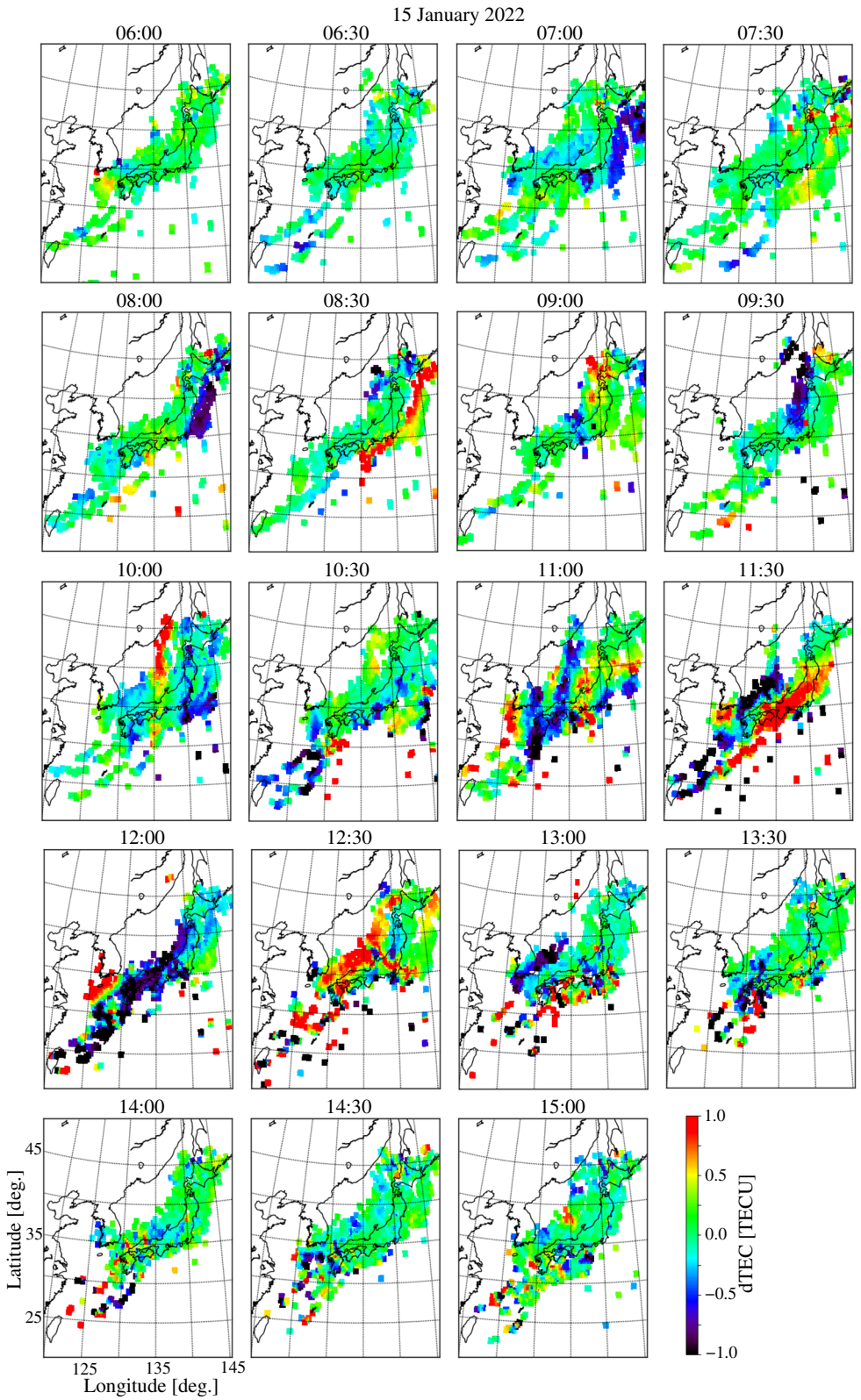

Fig. 2 TEC perturbation maps from 0600 to 1500 UT (1500 to 2400 JST) on 15 January 2022

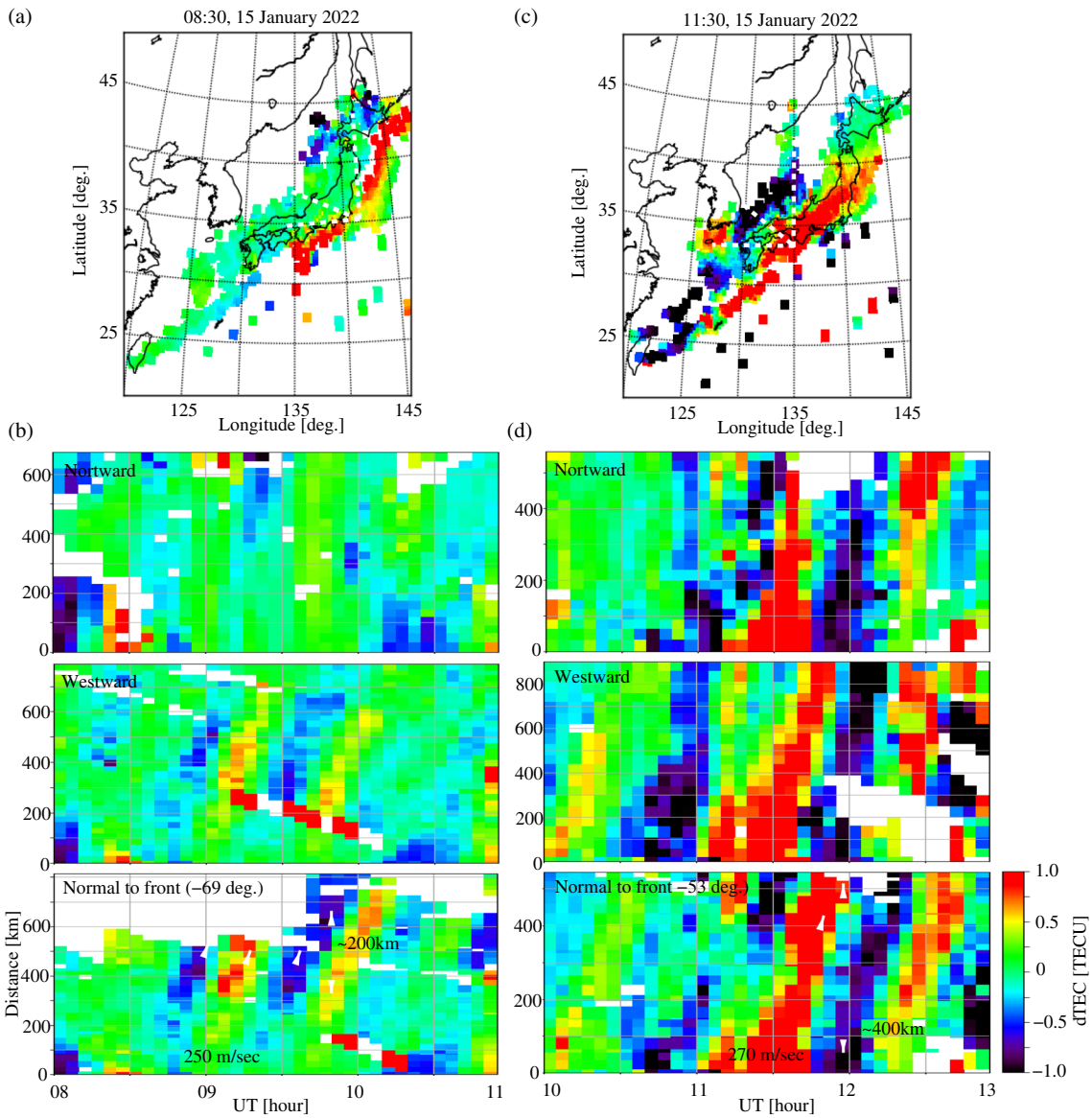

Fig. 3 **a** Perturbation component of TEC (dTEC) at 0830 UT (1730 JST) on 15 January 2022. **b** Keograms of dTEC along the white dashed lines in **a**, northward and westward directions, and the direction of the velocity from (37° N, 142° E). **c** dTEC at 1130 UT (2030 JST) on 15 January 2022. **d** Keograms of dTEC along the white dashed lines in **c**, northward and westward directions, and the direction of the velocity from (33° N, 137° E)

of the GEONET stations which are constrained by the shape of the Japanese archipelago. Figure 3b shows the keograms of dTEC from 0800 to 1100 UT along the lines in Fig. 3a. From the apparent velocity in the northward and westward direction from (37° N, 142° E), propagation velocity was estimated as 250 m s^{-1} in the direction −69° counter-clockwise from the north (WNW). According to the keogram in the direction of the propagation velocity, the wavelength was estimated as about 400 km. After 1000 UT, the speed seemed to slow down. Similar ionospheric disturbances were observed until 1100 UT. After 1100 UT, another ionospheric disturbances with dTEC amplitude of more than ±1.0 TECU appeared. The amplitude is stronger than the first TID, but is still within the range of amplitudes of typical TIDs in the mid-latitude region. Figure 3d shows the keograms of dTEC along the lines in Fig. 3c from 1000 to 1300 UT. In the same way as the first TID, the propagation velocity is estimated as 270 m s^{-1} in the direction −53° counter-clockwise from the north (NW). According to the keogram along the direction of the propagation velocity from (33° N,

135° E), the wavelength is estimated as about 800 km. The wavelengths of the first and second TIDs are within the range of the medium-scale traveling ionospheric disturbance (MSTID).

Figure 4 shows the series of ROTI maps over Japan from 0600 to 1500 UT [1500 to 2400 Japan Standard Time (JST)]. (A movie of the time evolution of ROTI maps with 5-min time step is included in Additional file 2). The distributions of IPPs may be slightly different from those of dTEC maps, because ROTI needs only 5 min before the value is obtained, while it takes 1 h for dTEC. The ROTI structures were matched with the dTEC structures of the first TID. In contrast, the second TIDs which started to be observed from 1100 UT did not accompany ROTI enhancement structures corresponding to the dTEC structure. ROTI enhancements are observed in a limited region.

Figure 5 shows the location of Hunga Tonga-Hunga Ha'apai in the azimuthal equidistant map with its center at Tokyo (35.69° N, 139.78° E), Japan. The surface distance between Tokyo and Hunga Tonga-Hunga Ha'apai is about 7800 km. Hunga Tonga-Hunga Ha'apai is in the azimuth direction of 135° clockwise from the north center of Japan.

For the TIDs started to be observed around 0700 UT which is about 3 h after the eruption of Hunga Tonga-Hunga Ha'apai, the arrival is too early, if they are caused by the atmospheric acoustic wave, because it would take roughly about 7 h. They might be caused by the atmospheric shock waves which propagates faster than the acoustic wave. Afraimovich et al. (2001) showed that atmospheric waves with phase velocity of 1100–1300 m s^{-1} were generated by earthquakes. They might also be caused by acoustic waves propagating in the thermosphere where the acoustic velocity is higher than the lower atmosphere. However, the propagation velocity of the TIDs was not so fast as the mean velocity estimated by the time difference from the eruption to the arrival. Another possibility is that the TIDs associated with electric field in the conjugate hemisphere might be mapped over Japan. The magnetic conjugate points of Japan is located over Australia which is located to the west of Hunga Tonga-Hunga Ha'apai. For example, the conjugate point of this TID (37° N, 142° E) is (21.03° S, 140.46° E). It is about 4600 km from Hunga Tonga-Hunga Ha'apai which is in the azimuth angle of 98° clockwise from the north. If the atmospheric waves induce oscillating electric field which could be generated by the E region dynamo process because it was in the daytime and are mapped over Japan, the shorter arrival time and propagation time could be explained.

Other sources which are not related to the eruption cannot be excluded by this analysis only. In the daytime in the winter in the northern hemisphere, TIDs associated with atmospheric gravity waves. However, their typical propagation direction is northward and different from what is observed for the first TID (Otsuka et al. 2021). It should be noted that the TID activity on the previous day (14 January 2022) was low and no clear TIDs were observed. TIDs are also induced by geomagnetic activity. Indeed, it was in a recovery phase of a moderate magnetic storm commenced on 14 January 2022. The Kp index on 15 January 2022 was not high ($2–4^{+}$). TIDs associated with magnetic storms are usually associated with heating of the thermosphere in the auroral region and propagate equatorward. Therefore, the first TID is not likely to be associated with geomagnetic activities. To understand the cause of this TIDs, observations between Hunga Tonga-Hunga Ha'apai and Japan are necessary. There are some GNSS stations in the Pacific Ocean by International GNSS Service (IGS). Although the number of stations are limited, data from IGS stations between Tonga and Japan would help understanding the propagation mechanisms. The first TID is rich in irregularities, as seen in ROTI maps, though it is still in daytime. Usually, the daytime TIDs caused by atmospheric gravity waves do not accompany ionospheric irregularities. It is unusual for daytime TIDs to accompany irregularities. This indicates that the atmospheric waves, if it is the cause of the TID, included turbulence which could generate turbulent structure of the ionospheric plasma. If the TID was associated with the electric field mapped from the magnetic conjugate points, the irregularities could be caused by electrodynamic plasma instability processes.

The second TIDs started to be observed after 1100 UT which is about 7 h after the eruption may be associated with the atmospheric acoustic waves. The propagation direction is consistent with the direction of Hunga Tonga-Hunga Ha'apai from Japan. It should be noted that surface pressure changes are observed around 1130 UT along the pacific coast of Japan as mentioned above. One of the interesting phenomena associated with the eruption was the abnormal enhancement of the tide level at the coast of Japan, while it was not so much at the Pacific islands. One of the potential mechanism is the effects of atmospheric waves on the sea surface, but evidences are limited. The observed TIDs with two different characteristics may add some information to understand the mechanisms of the abnormal tide level enhancement.

The ionospheric irregularities represented by ROTI are distributed not all over the second TIDs, but in a limited region as it can be seen ROTI map at 1130 UT. Ionospheric irregularities did not exist all over the TIDs, but exist in the limited region centered around (37° N, 135° E) with width of ±4° in latitude and longitude. In the nighttime, MSTIDs which are associated

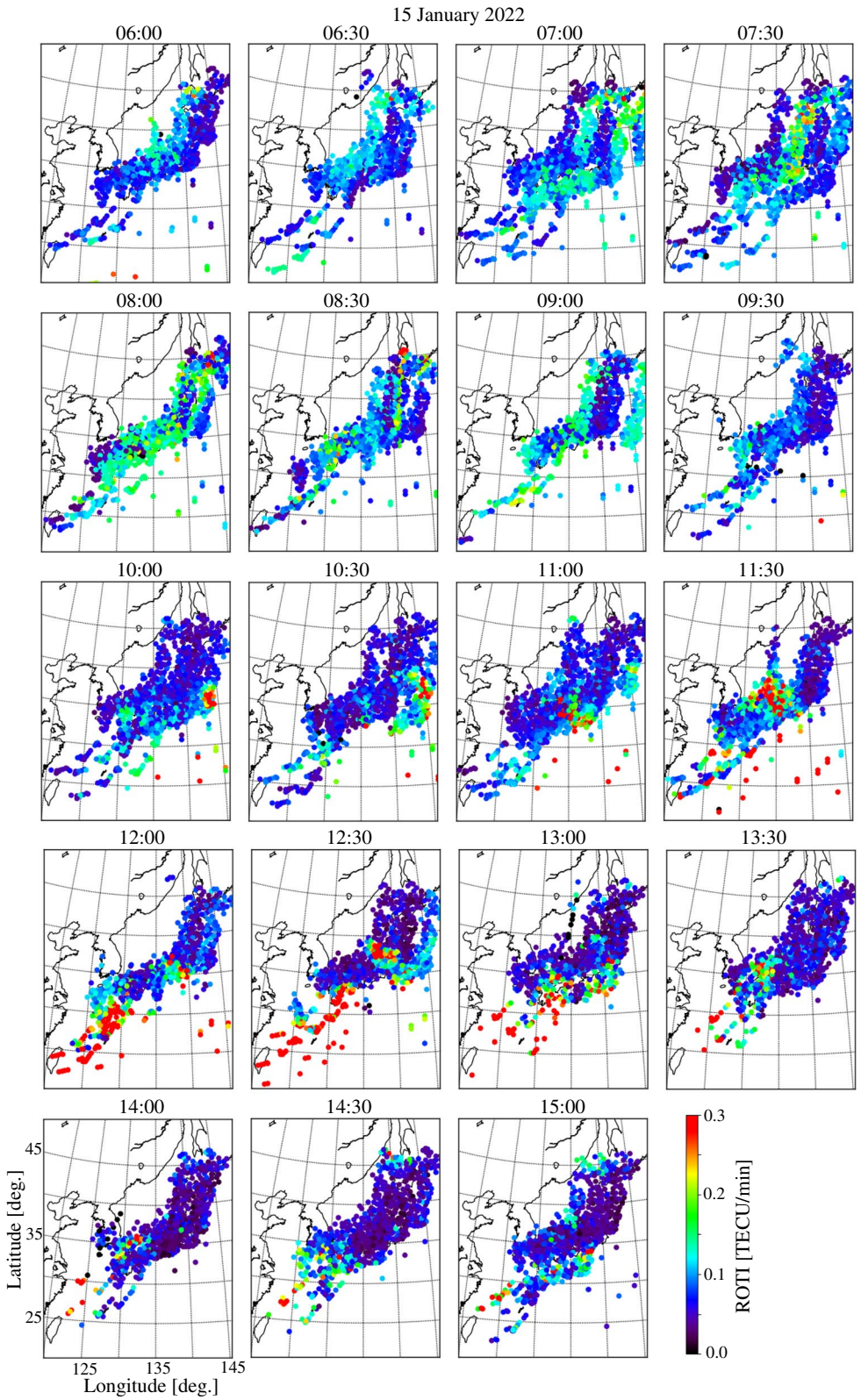

Fig. 4 ROTI maps from 0600 to 1500 UT (1500 to 2400 JST) on 15 January 2022

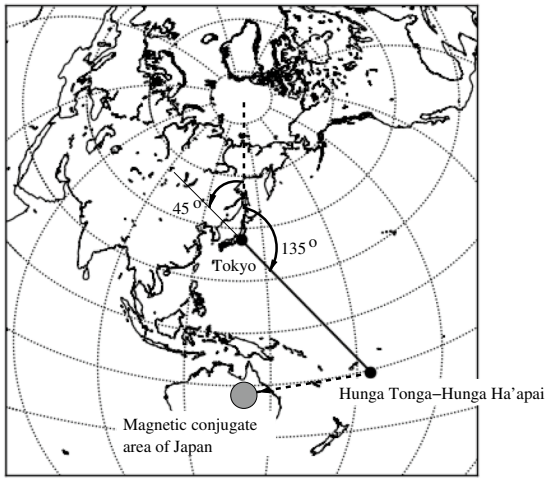

Fig. 5 Relative locations between Tokyo, Japan and Hunga Tonga-Hunga Ha'apai. The distance and direction are correct only from the center of the map

with the Perkins-type plasma instability accompanies ionospheric irregularities, but have same structures as MSTIDs. In the case of the current study, a region of ROTI enhancement appeared at the eastern edge of the coverage around 1000 UT and moved westward were distributed in the area where the two observed TIDs intersect each other. Two atmospheric waves interacted to generate small-scale waves and hence the ionospheric plasma structure becomes irregular. Other sources are not related to the eruption. As mentioned above, a moderate magnetic storm was going on. The observed structure of the region of ROTI enhancement looks similar to the storm-induced plasma stream observed in the low to mid-latitude region during magnetic storms (Maruyama et al. 2013), though it is usually observed strong geomagnetic storms. More studies are necessary to distinguish the effects of eruption from the magnetic storm.

From the viewpoint of GNSS applications, spatial variations of ionospheric TEC associated with the TIDs could degrade GNSS applications based on the differential GNSS technique. Even with the variation of ± 1 TECU, precise positioning systems which utilize carrier-phase measurements may be impacted, because the ionospheric delay of 1 TECU at the GPS L1 frequency is 0.16 *m* and comparable to the wavelength of the signals at the frequency, 0.19 *m*. The amplitude of the TIDs are within the range of those of typical MSTIDs, but the observed TIDs are associated with ROTI enhancements. Ionospheric irregularities which causes fluctuation of TEC represented by ROTI could further degrade performance of GNSS-based precise positioning systems by making differential GNSS difficult and signal tracking difficult. Real-time and wide-area monitoring of the ionospheric disturbances would be useful for accurate, stable, and reliable operations of GNSS-based systems.

Conclusions

By using the dense GNSS receiver network data in Japan, TIDs were observed following the eruption of Hunga Tonga-Hunga Ha'apai on 15 January 2022. Two types of TIDs with different characteristics were observed. The first one arrived at Japan which are located about 7800 km away from Hunga Tonga-Hunga Ha'apai about 3 h after the eruption. The amplitude was about ± 0.5 TECU. The wavefronts was in the NNE–SSW direction and propagated in the WNW direction ($-69°$ counter-clockwise from the north) at 250 m s^{-1}. The wavelength was estimated as 400 km. The second one arrived at Japan about 7 h after the eruption. The amplitude was about ± 1.0 TECU. The wavefronts was in the NE–SW direction and propagated in the NW direction ($-53°$ counter-clockwise from the north) at 270 m s^{-1}. The wavelength was longer than the first one and was estimated as 800 km. The first one were associated with ionospheric irregularities represented by ROTI. In contrast, the second one did not have irregularities all over the TIDs, but may be related to the geomagnetic storm which was going on. Further studies are necessary to distinguish the effects of the eruption and the geomagnetic storm. The arrival of the first TID was too early for the atmospheric acoustic waves to arrive. Mapping of the electric field from the magnetic conjugate points should be investigated. The arrival of the second TIDs approximately coincided with the arrival of surface pressure enhancement. To understand the mechanisms of the TIDs, further studies with wide-area observations as well as numerical calculations are necessary, and could help understanding the interactions of the atmosphere and sea surface, and eventually the abnormal enhancement of tide level around Japan. TIDs and ionospheric irregularities could be threats to GNSS-based systems especially for those which utilize carrier-phase measurements. Real-time and wide-area monitoring of the ionospheric disturbances would be useful for accurate, stable, and reliable operations of GNSS-based systems.

Abbreviations

dTEC: Delta total electron content; GEONET: GNSS Earth Observation NETwork; GNSS: Global Navigation Satellite System; GPS: Global Positioning System; IPP: Ionospheric Pierce Point; JST: Japan Standard Time; ROTI: Rate of TEC Index; TEC: Total electron content; TECU: Total electron content unit; UT: Universal time.

Supplementary Information

The online version contains supplementary material available at https://doi.org/10.1186/s40623-022-01619-0.

Additional file 1. A movie of the time evolution of the dTEC maps with 5 minutes time step from 0000 to 1500 UT.

Additional file 2. A movie of the time evolution of the ROTI maps with 5 minutes time step from 0000 to 1500 UT.

Acknowledgements
GEONET is operated and maintained by the Geospatial Information Authority of Japan. The Kp index data were provided by German Research Centre for Geoscience (GFZ) Potsdam.

Author contributions
SS designed this study, analyzed the data by using his developed continuously operating dTEC and ROTI analysis system, and interpreted the results. The author read and approved the final manuscript.

Funding
This study was partly supported by Grant-in-Aid for Scientific Research (B) (JP24340120) and Grant-in-Aid for Challenging Exploratory Research (JP26630182) by Japan Society for the Promotion of Science (JSPS) and the Ministry of Education, Culture, Sports, Science and Technology (MEXT) of Japan.

Availability of data and materials
The dTEC and ROTI maps are available at https://www.enri.go.jp/cnspub/susaito/rocket/. The Kp index data are available at https://www.gfz-potsdam.de/en/kp-index/.

Declarations

Competing interests
The authors declare that they have no competing interests.

Received: 27 January 2022 Accepted: 2 April 2022
Published online: 21 April 2022

References

Afraimovich EL, Perevalova NP, Plotnikov AV, Uralov AM (2001) The shock-acoustic waves generated by earthquakes. Annales Geophysicae 19:395–409
Cheng K, Huang YN (1992) Ionospheric disturbances observed during the period of Mount Pinatubo eruptions in June 1991. J Geophys Res 97(A11):16995–17004
Maeda J, Heki K (2014) Two-dimensional observations of midlatitude sporadic E irregularities with a dense GPS array in Japan. Radio Sci 49:28–35. https://doi.org/10.1002/2013RS005295
Maruyama T, Shinagawa S (2014) Infrasonic sounds excited by seismic waves of the 2011 Tohoku-oki earthquake as visualized in ionograms. J Geophys Res Space Phys 119:4094–4108. https://doi.org/10.1002/2013JA019707
Maruyama T, Tsugawa T, Kato H, Ishiii M, Nishioka M (2012) Rayleigh wave signature in ionograms induced by strong earthquakes. J Geophys Res Space Phys 117:A08306. https://doi.org/10.1029/2012JA017952
Maruyama T, Ma G, Tsugawa T (2013) Storm-induced plasma stream in the low-latitude to midlatitude ionosphere. J Geophys Res Space Phys 118:1–11. https://doi.org/10.1002/jgra.50541
Ogawa T, Kumagai H, Shinno K (1982) Ionospheric disturbances over Japan due to the 18 May 1980 eruption of Mount St. Helens. J Atmos Terr Phys 44:863–868
Otsuka Y, Kotake N, Tsugawa T, Shiokawa K, Ogawa T, Effendy Saito S, Kawamura M, Maruyama T, Hemmakorn N, Komolmis T (2006) GPS detection of total electron content variations over Indonesia and Thailand following the 26 December 2004 earthquake. Earth Planets Space 58:159–165
Otsuka Y, Shinbori A, Tsugawa T, Nishioka M (2021) Solar activity dependence of medium-scale traveling ionospheric disturbances using GPS receivers in Japan. Earth Planets Space 73:22. https://doi.org/10.1186/s40623-020-01353-5
Park J, Grejner-Brzezinska DA, Von Frese RB, Morton J (2014) GPS discrimination of traveling ionospheric disturbances from underground nuclear explosions and earthquakes. NAVIGATION J Inst Navig 61:125–134. https://doi.org/10.1002/navi.56
Pi X, Mannucci AJ, Lindqwister UJ, Ho CM (1997) Monitoring of global ionospheric irregularities using the worldwide GPS network. Geophys Res Lett 24:2283–2286. https://doi.org/10.1029/97GL02273
Saito A, Fukao S, Miyazaki S (1998) High resolution mapping of TEC perturbations with the GSI GPS network over Japan. Geophys Res Lett 25:3079–3082
Saito A, Tsugawa T, Otsuka Y, Nishioka M, Iyemori T, Matsumura M, Saito S, Chen CH, Goi Y, Choosakul N (2011) Acoustic resonance and plasma depletion detected by GPS total electron content observation after the 2011 off the Pacific coast of Tohoku Earthquake. Earth Planets Space 63:863–867
Saito S, Yoshihara T, Yamamoto M (2014) Real time ionospheric disturbance analysis and monitoring with GEONET real time data. In: Proceedings of the 2014 international technical meeting of the Institute of Navigation (ION ITM 2014), San Diego, California, January 2014. pp 720–724
Saito S, Hosokawa K, Sakai J, Tomizawa I (2021) Study of structures of the sporadic E layer by using dense GNSS network observations. NAVIGATION J Inst Navig 68:751–758. https://doi.org/10.1002/navi.454
Savastano G, Komjathy A, Verkhoglyadova O, Mazzoni A, Crespi M, Wei Y, Mannucci AJ (2017) Real-time detection of tsunami ionospheric disturbances with a stand-alone GNSS receiver: a preliminary feasibility demonstration. Sci Rep 7:46607. https://doi.org/10.1038/srep46607
Tsugawa T, Saito A, Otsuka Y, Nishioka M, Maruyama T, Kato H, Nagatsuma T, Murata KT (2011) Ionospheric disturbances detected by GPS total electron content observation after the 2011 off the Pacific coast of Tohoku Earthquake. Earth Planets Space 63:875–879

Publisher's Note